Title
SEARCH FOR TIGHT-HANDED CURRENTS IN MUON DECAY

Author
Carr, J.

Publication Date
1983-06-01

Lawrence Berkeley Laboratory
UNIVERSITY OF CALIFORNIA

Physics, Computer Science & Mathematics Division

Submitted to Physical Review Letters

SEARCH FOR RIGHT-HANDED CURRENTS IN MUON DECAY

J. Carr, G. Gidal, B. Gobbi, A. Jodidio,
C.J. Oram, K.A. Shinsky, H.M. Steiner, D.P. Stoker,
M. Strovink, and R.D. Tripp

June 1983

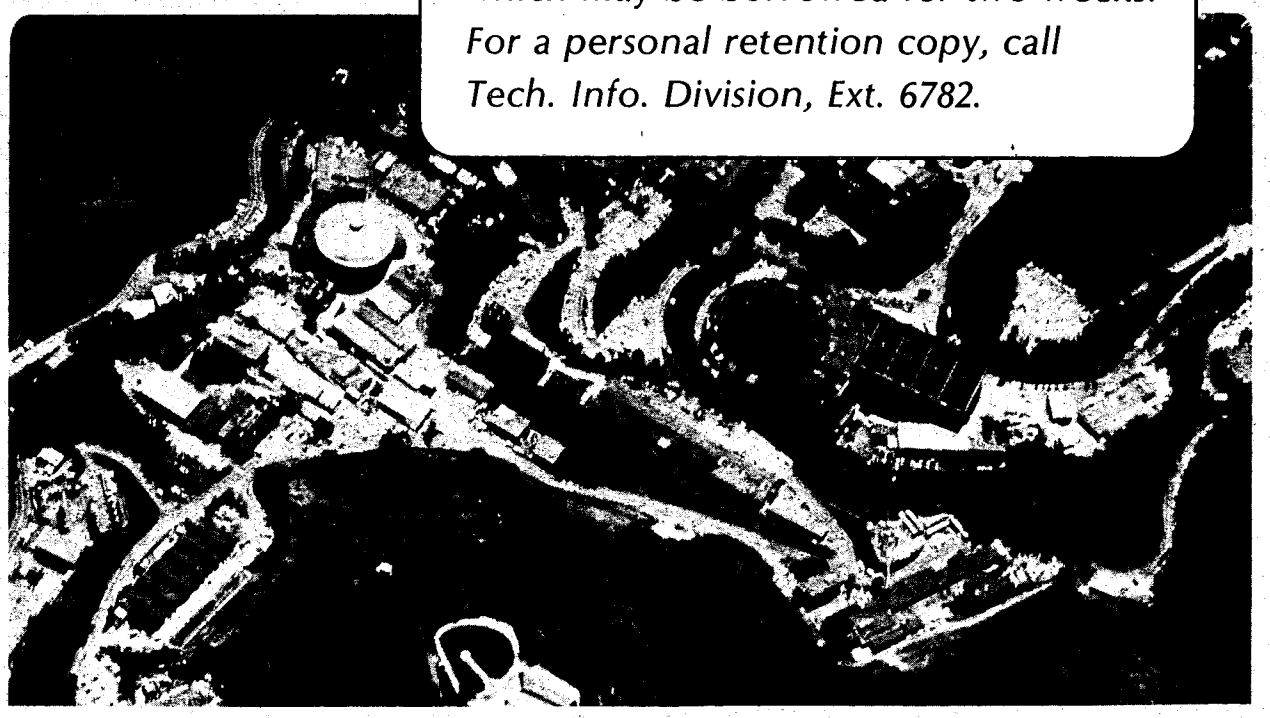

Prepared for the U.S. Department of Energy under Contract DE-AC03-76SF00098

DISCLAIMER

LBL-16183

SEARCH FOR RIGHT-HANDED CURRENTS IN MUON DECAY

J. Carr, G. Gidal, B. Gobbi[†], A. Jodidio, C.J. Oram[††], K.A. Shinsky,

H.M. Steiner, D.P. Stoker, M. Strovink, and R.D. Tripp

Lawrence Berkeley Laboratory and Department of Physics

University of California, Berkeley, California 94720

[†]Department of Physics, Northwestern University, Evanston, IL 60201

[††]Tri-University Meson Facility, Vancouver, B.C. V6T2A3, Canada

ABSTRACT

We report new limits on right-handed currents, based on precise measurement of the e^+ spectrum endpoint in μ^+ decay. Highly polarized muons from the TRIUMF "surface" beam were stopped in metal foils within a 1.1-T spin-holding longitudinal field or a 70-gauss spin-precessing transverse field. For the spin-held data, the (V-A) decay rate vanishes in the beam direction at the endpoint. Measurement of this rate sets the 90%-confidence limits $\xi P_\mu \delta/\rho > 0.9959$ and $M(W_R) > 380$ GeV, where W_R is the possible right-handed gauge boson.

If the $SU(2)_L \times U(1)$ gauge group in the standard electroweak model is extended e.g. to $SU(2)_L \times SU(2)_R \times U(1)$,[1] left-right symmetry at the Lagrangian level is restored with the addition of a right-handed gauge boson W_R. The dominance of left-handed charged currents at present energies could then arise from a W_L–W_R mass splitting which is tiny on the grand-unification scale. In these left-right symmetric theories, the physical bosons W_1 and W_2, with mass-squared ratio $\alpha = M^2(W_1)/M^2(W_2)$, are $W_1 = W_L \cos\zeta - W_R \sin\zeta$ and $W_2 = W_L \sin\zeta + W_R \cos\zeta$. Analyses[2,3] which neglect the kinematic effect of any ν_R mass obtain the strongest limits on α and the mixing angle ζ from muon and nucleon β decay.[4–9] Additional constraints are placed by model dependent calculations e.g. of the K_L^0–K_S^0 mass difference.[10] Present experimental bounds are displayed in Fig. 1. To improve the experimental sensitivity, we have precisely measured the high-momentum region of the e^+ spectrum in polarized μ^+ decay. The small bold ellipse in Fig. 1 is the limit set by the new data presented here.

The stopped μ^+ decays of interest are those which emit e^+ near the momentum-spectrum endpoint $x = p_e/p_e(max) = 1$, and also near $\theta = 0$, where π–θ is the angle between $\hat{p}_e$ and the direction of μ^+ polarization P_μ. Relative to that for unpolarized muons, the decay rate is

$$R(x,\theta) = 1 - \frac{1-2\tilde{x}-\tilde{\delta}+4\tilde{x}\tilde{\delta}}{1+2\tilde{x}-\tilde{\rho}+4\tilde{x}\tilde{\rho}}\ \xi P_\mu \cos\theta\ , \qquad (1)$$

where $\tilde{x} = 1-x$, $\tilde{\delta} = 1-4\delta/3$, $\tilde{\rho} = 1-4\rho/3$, and ξ, δ, and ρ are the usual muon decay parameters.[11] (Radiative corrections [11] and the finite electron mass are included in the actual analysis but neglected in (1) above.) At the endpoint, $R(1,0) = 1-\xi P_\mu \delta/\rho$, and in the (V-A) limit, $R(x\to 1,\theta\to 0) \approx 6-4x-P_\mu-\cos\theta$. For a μ^+ beam derived from π^+ decay at rest, θ becomes the angle between the e^+ and μ^+ momenta. Then, in left-right symmetric theories,[2] $P_\mu \approx 1-2(\alpha+\zeta)^2$, and the endpoint decay rate $R(1,0) \approx 2(2\alpha^2 + 2\alpha\zeta + \zeta^2)$ constrains both α and ζ.

This experiment is made possible by the nearly complete polarization of a μ^+ beam derived from π^+ decay at rest near the surface of the production target.[12] The $M13$ beam[13] at the Tri-University Meson Facility (TRIUMF) cyclotron produces 15,000 29.5-MeV/c μ^+/sec within a 1% momentum bite and a 12×10 mm spot. The 2% contamination of prompt ("cloud") μ^+ from π^+ decay in flight

is rejected by requiring the μ^+ to be produced well within the 43-nsec interval between proton bursts.

The apparatus is shown in Fig. 2. After traversing 50 mg/cm^2, beam μ^+ are stopped by target foils of $\geq$99.99% pure Al (155 mg/cm^2), Cu (233 mg/cm^2), Ag (275 mg/cm^2), and Au (233 mg/cm^2). The high free-electron concentration in these metals screens the stopped μ^+ from prolonged spin-spin coupling to particular electrons, which otherwise would lead to its depolarization. A 1.1-T longitudinal field ($B_{//}$) is also applied to preserve the stopped μ^+ spin direction. During alternate hourly runs the longitudinal field is nulled to within $\pm$3 gauss and a 70-gauss transverse field ($B_{\perp}$) is substituted. This precesses the μ^+ spin about a vertical axis so that its time-averaged polarization is zero. Downstream of the target the decay e^+ is focused by a 0.5 T-m solenoidal field lens. The septum between the target and solenoid bore decouples the focal length from the choice of target field orientation.

The decay e^+ is momentum-analyzed by an NMR-monitored cylindrical dipole magnet having a central field of 0.32 T. Low-mass driftchambers using methane gas are located near its conjugate foci, and the intervening volume is evacuated. The dispersion $\Delta p/p$ was measured to be 1.07%/cm by passing e^+ beams of different momenta through the spectrometer. The combined system of field lens and positron spectrometer has an acceptance of 250 msr and a momentum bite of $\pm$20%; in the analysis described below, these were restricted to 160 msr and $\pm$8%.

The trigger requires the signature of a beam particle stopping in the foil target, in delayed (0.2 – 10 μsec) coincidence with that of a decay positron passing through the spectrometer. Events with an extra beam particle arriving between the μ^+ stop and decay are tagged and rejected later. The data reported here are based on 3.5×10^6 triggers from the initial run. An additional 10^7 triggers were collected later in 1982.

Incoming μ^+ tracks were reconstructed using $P1$ and $P2$. Nearly straight e^+ track segments were found separately in the horizontal and vertical projections of three groups of wire chamber planes:

($P3$, $D1$, $D2$); $D3$; and $D4$ (Fig. 2). All possible combinations of hits were considered, and tracks in all six segments were found in 99% of the triggers. Of these, 95% had hit multiplicities corresponding to a single track; the remainder were rejected. Projections of the track segments were required to agree at the target, in the bore of the solenoid, and in position and vertical slope in the dipole. Track segment residuals were used to dynamically fine-tune the driftchamber space-time calibration, producing residuals of $\leq 250\ \mu$ in the spectrometer chambers $D3$ and $D4$.

The hits found in $P1$ through $D2$ were then fitted to curved trajectories based on the first-order optics of cylindrically symmetric fields. The μ^+ and e^+ polar angles θ_μ and θ_e with respect to the beam axis at the target were thereby determined with resolutions of 20 and 10 mrad, respectively. Monte Carlo simulation based on higher-order field optics confirms the accuracy of this procedure to within an uncertainty of ± 0.0005 in $\cos\theta_\mu$ and $\cos\theta_e$. For the $B_{//}$ data the transverse component of the μ^+ spin precesses about the beam axis too rapidly to be followed. Thus for $\cos\theta = -\hat{P}_\mu \cdot \hat{p}_e$ in Eq. 1 we substitute $\cos\theta_\mu \cos\theta_e$, which is equivalent in an average over many events.

The e^+ momentum was obtained by taking the sum of the horizontal coordinates at the conjugate foci of the 98° horizontally focussing spectrometer magnet. Using the momentum, deviation from the median plane, and impact parameter with respect to the magnet axis as parameters, this sum was empirically corrected to second order, based primarily on the endpoint position in $B_\perp$ data. The sharp edge at $x = 1$ in Fig. 3(a) exhibits a gaussian resolution which is less than 0.2% rms, with a rounded shoulder due to straggling in the 180 mg/cm^2 of material upstream. We have dropped events with $x < 0.92$ and $\cos\theta < 0.975$, which have low statistical power. After conservative fiducial cuts the final distributions in Fig. 3 retain 7.5% of the raw triggers. We have checked that any reasonable variation of the cuts would negligibly affect the result.

Fitting proceeds in two stages. The $B_\perp$ data in Fig. 3(a) are fitted to the radiatively corrected spectrum expected[11] for unpolarized μ^+ decay, smeared by a sum of gaussian resolution functions and by the expected e^+ energy-loss straggling. The $B_{//}$ spectrum in Fig. 3(b) can be represented as the shape expected from pure (V-A) and $P_\mu = \cos\theta = 1$, with a small admixture of the unpolarized

spectrum in Fig. 3(a). This unpolarized fraction is essentially equal to $1-(\xi P_\mu \delta/\rho)<\cos\theta>$. To fit this fraction, we use the $B_\perp$ fit to fix the x resolution, x acceptance, and edge position $x=1$, but allow the acceptance for $B_{//}$ data relative to that for $B_\perp$ data to vary linearly with x. This allows for the (<2%) difference in angular acceptance caused by the different field configuration near the target. Using data with partly polarized cloud μ^+, we have checked that the $x=1$ calibration is consistent for $B_{//}$ and $B_\perp$ fields. In the resulting curve in Fig. 3(b), the slight kink near $x=1$ reflects the small fitted unpolarized fraction, which arises mostly from the measured value $<\cos\theta> = 0.9862$ for these data.

The result reported here is based on this same fitting procedure carried out for data in each of five bins in $\cos\theta$. The subdivision checks that the results of these fits are consistent with a linear dependence upon $<\cos\theta>$. Separate fits for each of the four stopping target materials give values of $\xi P_\mu \delta/\rho$ which are statistically consistent ($\chi^2 = 2.1$), with a combined statistical error of ± 0.0015. Within statistical errors the result is also independent of the time of muon decay.

Because the measured values of $\cos\theta_\mu \cos\theta_e$ are systematically too high due to Coulomb scattering in the production and stopping targets, an estimated correction of $+0.0012 \pm 0.0005$ has been applied to all fitted $\xi P_\mu \delta/\rho$. Table I summarizes the major sources of systematic error. All other sources contribute less than 10^{-4}. In principle the systematic errors should not be correlated; in quadrature they add to ± 0.0018. We have made no correction for unknown sources of μ^+ depolarization either along the beam or in the stopping target. Since such effects can only decrease the apparent result, we therefore quote the limit $\xi P_\mu \delta/\rho > 0.9959$ (90% confidence). The corresponding limits on the mass and mixing parameters α and ζ are represented by the small bold contour in Fig. 1. In particular, for infinite W_R mass $|\zeta| < 0.045$; for any mixing angle $M(W_R) > 380$ GeV; and for zero mixing angle $M(W_R) > 450$ GeV.

We are indebted to the entire TRIUMF management and staff for their splendid support of this experiment. In its early stages we benefited from discussions with J. Brewer, R. Cahn, K. Crowe, K. Halbach, and W. Wenzel, and from the technical contributions of C. Covey, R. Fuzesy, F.

Goozen, P. Harding, M. Morrison, and P. Robrish. This research was supported in part by the U.S. Department of Energy, Division of Basic Energy Sciences, Office of Energy Research under contracts DE-AC03-76SF00098 and AC02-ER02289.

References

1. J.C. Pati and A. Salam, Phys. Rev. *D11*, 566 and 2558 (1975); R.N. Mohapatra and J.C. Pati, Phys. Rev. *D12*, 1402 (1975).

2. M.A.B. Bég, R.V. Budny, R. Mohapatra, and A. Sirlin, Phys. Rev. Lett. *48*, 1252 (1977).

3. B.R. Holstein and S.B. Treiman, Phys. Rev. *D16*, 2369 (1977).

4. The primary input to the world average is V.V. Akhmanov et al., Yad. Fiz. *6*, 316 (1967).

5. The primary input to the world average is J. Peoples, Nevis Cyclotron Report No. 147 (1966) (unpublished).

6. J. Van Klinken, Nucl. Phys. *75*, 145 (1966).

7. J. Van Klinken et al., Phys. Rev. Lett. *50*, 94 (1983).

8. D. Schreiber and F.T. Calaprice, private communication; D. Schreiber, Ph.D. Thesis, Princeton University, 1983 (unpublished). We calculated the contour plotted in Fig. 1 using $A(0) = 0.0363 \pm 0.0008$; ft ratio $= 1.797 \pm 0.002$. See also F.T. Calaprice et al., Phys. Rev. Lett. *35*, 1566 (1975).

9. H. Abramowicz et al., Z. Phys. *C12*, 225 (1982).

10. G. Beall, M. Bander, and A. Soni, Phys. Rev. Lett. *48*, 848 (1982); P. DeForcrand, Ph.D. Thesis, Univ. of Calif., Berkeley (1982), LBL-14692 (to be published).

11. F. Scheck, Phys. Lett. *C44*, 187 (1978); A.M. Sachs and A. Sirlin, in *Muon Physics*, Vol. II, V. Hughes and C.S. Wu, eds. (Academic Press, N.Y., 1975), p. 50.

12. A.E. Pifer et al., Nucl. Inst. Meth. *135*, 39 (1976).

13. C.J. Oram et al., Nucl. Inst. Meth. *179*, 95 (1981).

TABLE I.

Major sources of systematic error and their estimated contributions.

Source of systematic error	Error
Coulomb scattering in targets	± 0.0005
Correction of θ_μ and θ_e for bending in $B_{//}$ field at target	± 0.0010
Smearing of θ_μ and θ_e due to detector resolution and scattering	± 0.0006
Possible shift in θ_e due to random hits and inefficiencies in $D1$ and $D2$	± 0.0005
Method of averaging $<\cos\theta>$	± 0.0004
Difference in $x=1$ edge calibration between $B_\perp$ and $B_{//}$ data	± 0.0008
Normalization of $B_{//}$ relative to $B_\perp$ data	± 0.0007

Figure Captions

FIG. 1. Experimental 90%-confidence limits on the $W_{L,R}$ mass-squared ratio α and mixing angle ζ describing possible right-handed charged currents. The allowed regions are those which include $\alpha = \zeta = 0$. Muon-decay contours are derived from decay rate measurements at the spectrum end-point (bold, this experiment); the polarization parameter ξP_μ (dotted, Ref. 4); and the Michel parameter ρ (solid, Ref. 5). Nuclear β decay contours are obtained from the Gamow-Teller β polarization (dot-dashed, Ref. 6); the comparison of Gamow-Teller and Fermi β polarizations (long-dashed, Ref. 7); and the ^{19}Ne asymmetry $A(0)$ and ft ratio, assuming CVC (short-dashed, Ref. 8). Limits from the y distributions in νN and $\bar{\nu} N$ scattering (double lines, Ref. 9) are valid irrespective of the ν_R mass.

FIG. 2. Plan view of muon polarimeter. P1-P3 are proportional wire chambers, D1-D4 are driftchambers, and S1-S3 are scintillators. The trigger is T1·T2, where T1 is $P1 \cdot S1 \cdot P2 \cdot \overline{V1} \cdot \overline{P3} \cdot \overline{S2}$ at the μ^+ stopping time, T2 is $P3 \cdot S2 \cdot S3 \cdot \overline{P1} \cdot \overline{S1} \cdot \overline{V1} \cdot \overline{P2} \cdot \overline{V2}$ at the μ^+ decay time, and V1 and V2 are veto scintillators surrounding S1 and S2, respectively (not shown).

FIG. 3. Distributions (uncorrected for acceptance) in reduced positron momentum with the μ^+ spin (a) precessed and (b) held. Errors are statistical. The edge in (a) corresponds to a resolution with a gaussian part $<0.2\%$ rms. The fits are described in the text.

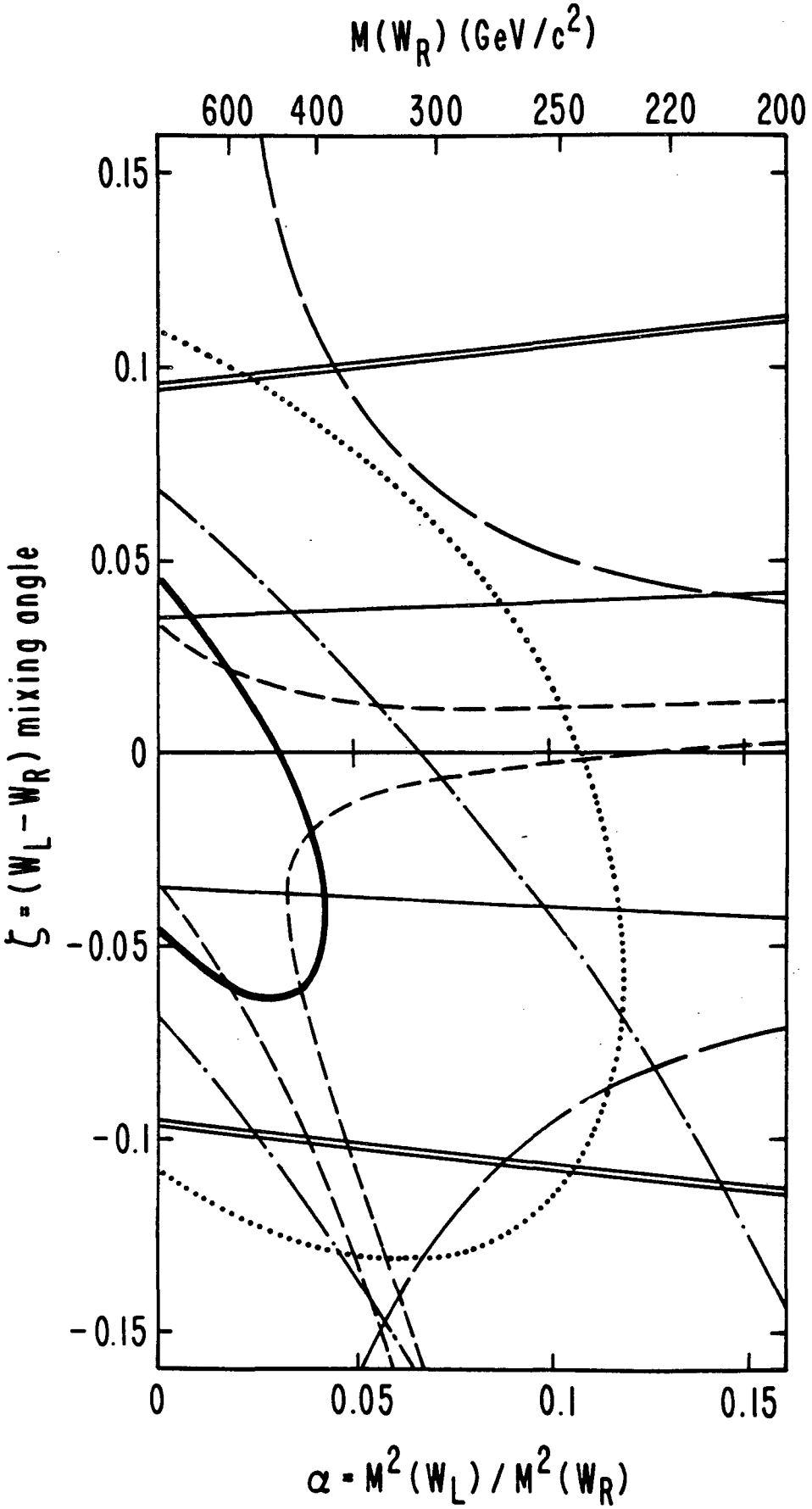

XBL 834-145

Fig. 1

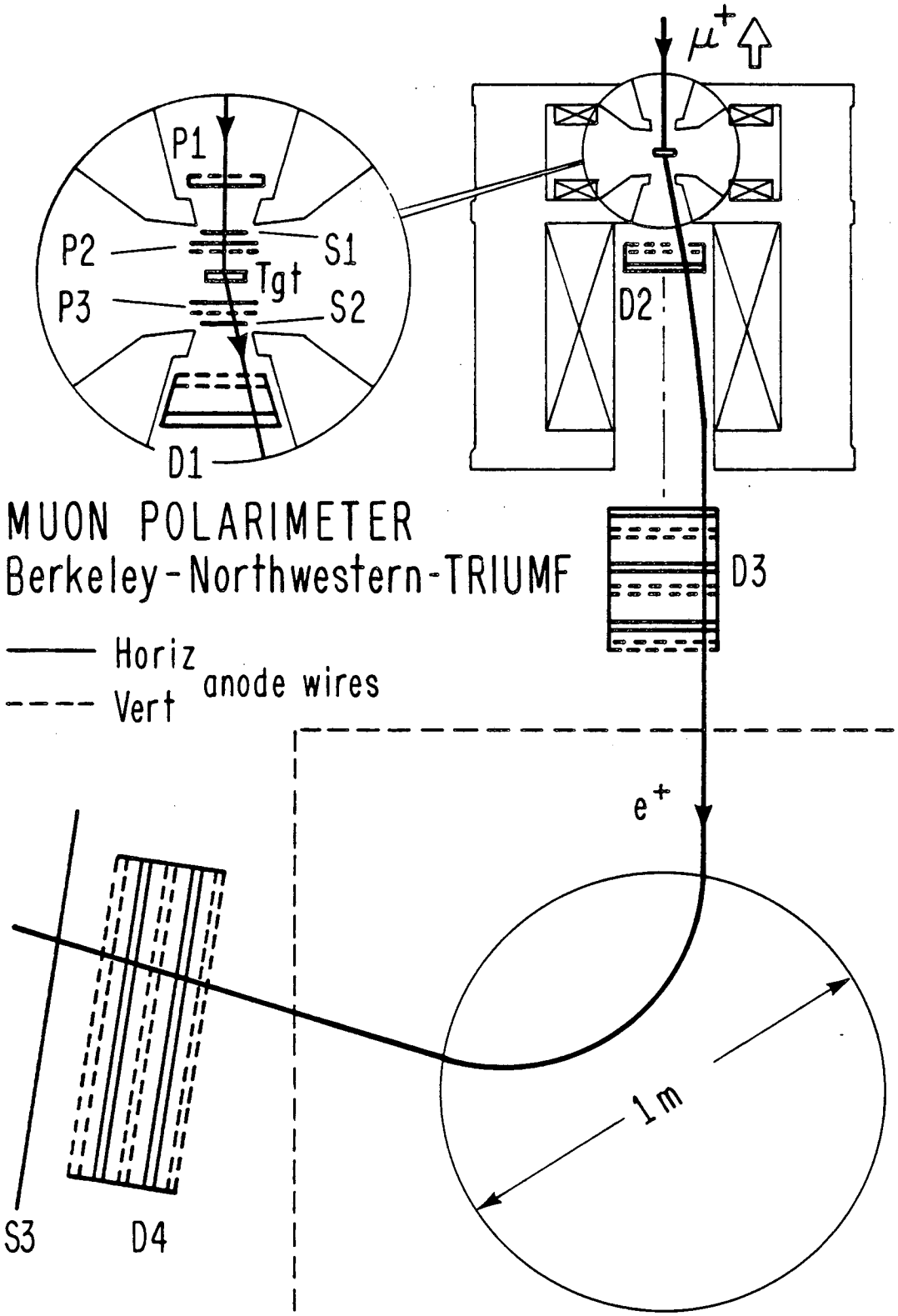

XBL 834-147

Fig. 2

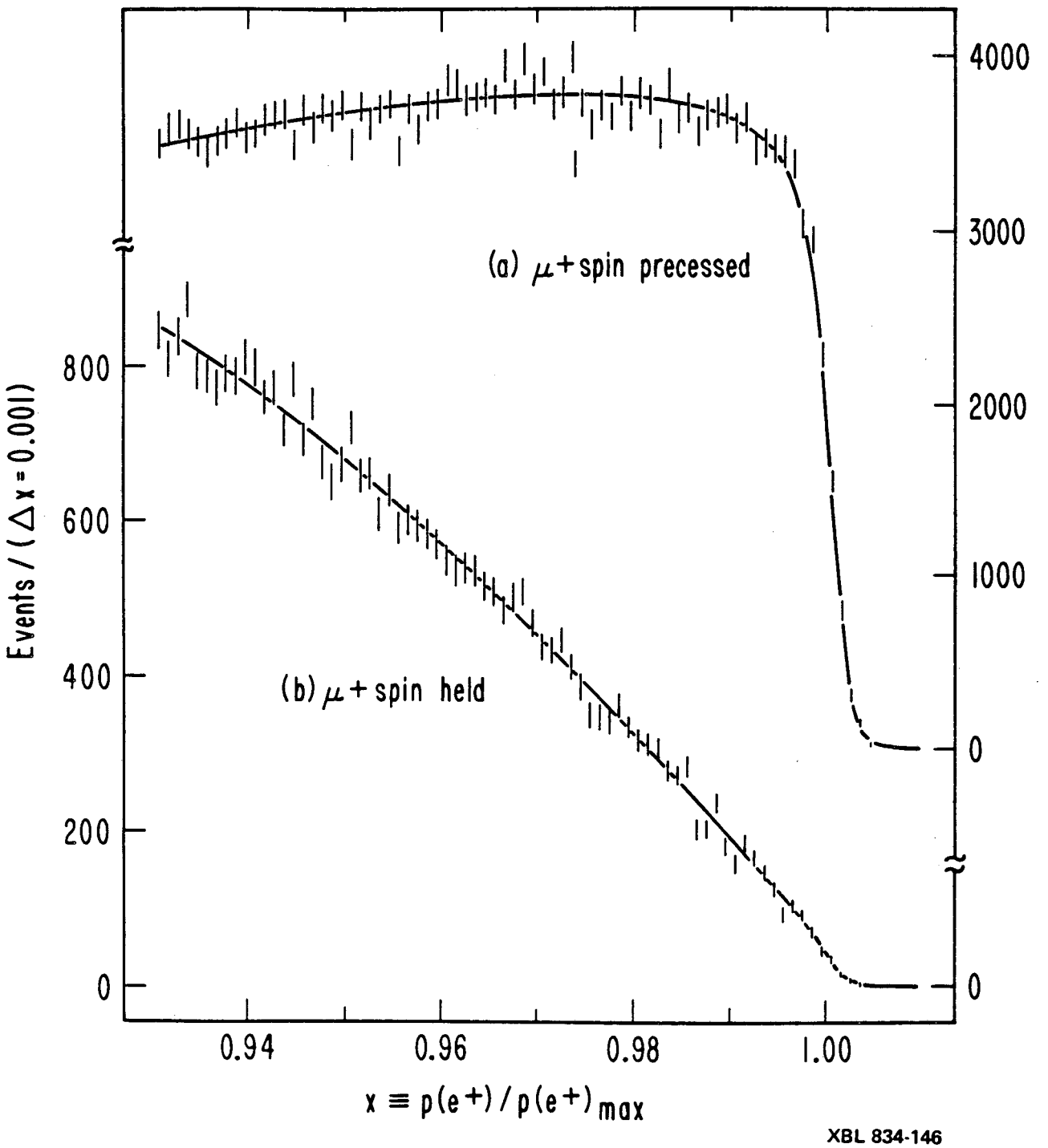
(a) μ+ spin precessed
(b) μ+ spin held
Events / (Δx = 0.001)
4000
3000
2000
1000
0
800
600
400
200
0
0.94
0.96
0.98
1.00
x ≡ p(e+) / p(e+)max
XBL 834-146

Fig. 3

This report was done with support from the Department of Energy. Any conclusions or opinions expressed in this report represent solely those of the author(s) and not necessarily those of The Regents of the University of California, the Lawrence Berkeley Laboratory or the Department of Energy.

Reference to a company or product name does not imply approval or recommendation of the product by the University of California or the U.S. Department of Energy to the exclusion of others that may be suitable.

TECHNICAL INFORMATION DEPARTMENT
LAWRENCE BERKELEY LABORATORY
UNIVERSITY OF CALIFORNIA
BERKELEY, CALIFORNIA 94720